

# Finding metastable skyrmionic structures via a metaheuristic perturbation-driven neural network

Qichen Xu,<sup>1,2</sup> I. P. Miranda\*,<sup>3</sup> Manuel Pereiro\*,<sup>3</sup> Filipp N. Rybakov,<sup>3</sup> Danny Thonig,<sup>4,3</sup> Erik Sjöqvist,<sup>3</sup> Pavel Bessarab,<sup>5</sup> Anders Bergman,<sup>3</sup> Olle Eriksson,<sup>3</sup> Pawel Herman,<sup>6,2</sup> and Anna Delin<sup>1,2</sup>

<sup>1</sup>*Department of Applied Physics, School of Engineering Sciences, KTH Royal Institute of Technology, AlbaNova University Center, SE-10691 Stockholm, Sweden*

<sup>2</sup>*SeRC (Swedish e-Science Research Center), KTH Royal Institute of Technology, SE-10044 Stockholm, Sweden*

<sup>3</sup>*Department of Physics and Astronomy, Uppsala University, Box 516, SE-75120 Uppsala, Sweden\**

<sup>4</sup>*School of Science and Technology, Örebro University, SE-701 82, Örebro, Sweden*

<sup>5</sup>*Department of Physics and Electrical Engineering, Linnaeus University, Hus Magna, Kalmar, SE-13077, Sweden*

<sup>6</sup>*Division of Computational Science and Technology, School of Electrical Engineering and Computer Science, KTH Royal Institute of Technology, AlbaNova University Center, SE-10691 Stockholm, Sweden*

(Dated: March 7, 2023)

Topological magnetic textures observed in experiments can, in principle, be predicted by theoretical calculations and numerical simulations. However, such calculations are, in general, hampered by difficulties in distinguishing between local and global energy minima. This becomes particularly problematic for magnetic materials that allows for a multitude of topological charges. Finding solutions to such problems by means of classical numerical methods can be challenging because either a good initial guess or a gigantic amount of random sampling is required. In this study, we demonstrate an efficient way to identify those metastable configurations by leveraging the power of gradient descent-based optimization within the framework of a feedforward neural network combined with a heuristic meta-search, which is driven by a random perturbation of the neural network's input. We exemplify the power of the method by an analysis of the Pd/Fe/Ir(111) system, an experimentally well characterized system.

## I. INTRODUCTION

In systems with many interacting entities, *e.g.*, a chain of amino acids forming a protein [1], a metal cluster [2], or a system of spins [3], the Hamiltonian and its corresponding potential energy surface (PES) can quickly become complex as the number of interacting particles increases. In the case of coupled spins, this complexity is expressed in the form of *rugosity* on the PES, driven by frustration or competing spin-spin interactions.

In such cases, finding the global minimum is usually a challenging task due to the non-convexity of the high-dimensional function that represents the PES [4]; in extreme frustration levels, such as in spin glasses, the problem of minimizing the energy function given by the spin Hamiltonian is known to be contained in the nondeterministic polynomial (NP-hard) class [5].

Not only the global minimum but also the numerous local minima can provide important information about a given system. In fact, many of these states corresponding to local minima can be very long-lived at finite temperatures and have significant consequences for the physical behavior of the system. Magnetic skyrmions are prime examples of such states. Depending on the intrinsic properties (interactions, geometry, anisotropy) and external conditions (field, temperature), skyrmions can emerge as metastable (excited) states in the configuration space, as confirmed by previous experiments [6–9]. For such

systems, when the spin Hamiltonian is properly parameterized by realistic values of interactions, Monte Carlo (MC) calculations [10] are often able to reproduce those metastable skyrmions [6, 7, 11].

Nevertheless, the more complex counterparts (*e.g.*, given in Ref. [12]), also metastable, are rarely and/or not systematically found in such MC simulations – as this is a method designed for finding the ground-state. Among other reasons, the importance of such theoretical predictions lies on the possibility of coexistence of those complex counterparts with skyrmions (or other analogous quasi-particles) in a single material. This condition has been pointed as a possible solution of the '0'-bit representation problem [13]: on the long time scales, the definition of the '0' bit of information as the absence of skyrmionic textures becomes problematic; in this case, the skyrmionic-gap positions cannot be precisely fixed and can change due to interparticle repulsion. Therefore, the need to find candidate metastable states in a rugged PES in a more systematic way requires another approach. To overcome this obstacle, metaheuristic searching algorithms are potential choices to efficiently produce advisable solutions with a high-dimensional search space [14].

Here, we propose a metaheuristic algorithm based on gradient-descent optimization within a neural network framework, parameterized to approximate the configuration of the atomistic spin vectors at the lattice sites and driven by random perturbations. The learning objective for the network is set to the minimization of the Hamiltonian. Importantly, by a random perturbation of the network's input, triggered by *a priori* knowledge condition, which includes physical insight and understanding

---

\* These two authors contributed equally

of the studied system, the algorithm can perform an iterative search for multiple energy minima.

We demonstrate our method for a model of a well-known frustrated system of interacting spins – the Pd/Fe/Ir(111) film. This system has been very thoroughly characterized experimentally and was one of the first studied systems containing two-dimensional magnetic skyrmions [15].

As a criterion dictated by prior knowledge, we have selected the maximization of the energy contribution from the Dzyaloshinskii-Moriya interaction (DMI), since this interaction is of central importance for skyrmion stability. With our method, we have identified and characterized many previously unknown skyrmions. For example, skyrmion-antiskyrmion pairs, various types of skyrmionium, (anti-)skyrmion bags with/without "limbs", and other states with varying degrees of similarity with known magnetic textures [12, 16–20]. Furthermore, we perform an analysis of the behavior and stability of the identified skyrmions at finite temperatures.

This work is organized as follows: in Section II, the newly designed algorithm called functional perturbation neural network, as well as a hybrid mode that combined it with Markov chain Monte Carlo (MCMC) are described. In Sec. III, the identified high-order antiskyrmions textures and their stability are discussed at finite temperatures. The manuscript concludes in Sec. IV.

## II. METHOD

### A. Metaheuristic perturbation-driven neural network

Currently, several algorithms exist that are useful for finding minima in complex potential energy surfaces, for example, Markov chain Monte Carlo (MCMC) based simulated annealing [21, 22] or the velocity projection energy minimization method [23, 24].

For many of these algorithms, it is often the case that the local minima it finds depend substantially on the initial state provided to the algorithm [25].

As conceptually shown in Fig. 1 (a), our method performs a meta-heuristic search for multiple local minima. The critical component of our approach is a universal approximator in the form of a single-hidden-layer feed-forward neural network with the loss function representing the PES [26–29]. In other words, the spin Hamiltonian is mapped to the loss function of the network driven by a random input (following the normal distribution  $X \sim \mathcal{N}(0, 1)$ ), considered as the initial condition for optimization. In particular, as shown in Fig. 1 (b), the spin configurations are parameterized by arbitrary weights in a neural network that can be systematically tuned to minimise the total energy of the system repre-

sented by the Hamiltonian (the loss function):

$$\begin{aligned} \mathcal{L}(S_1, S_2 \dots S_n) &= \mathcal{H}(S_1(X), S_2(X) \dots S_n(X)) \\ &= \mathcal{H}_{\text{Heis}}(S) + \mathcal{H}_{\text{DM}}(S) \\ &\quad + \mathcal{H}_{\text{Zeeman}}(S) + \mathcal{H}_{\text{ani}}^U(S) \\ &= - \sum_{i \neq j} J_{ij} \mathbf{S}_i \cdot \mathbf{S}_j - \sum_{i \neq j} \mathbf{D}_{ij} \cdot (\mathbf{S}_i \times \mathbf{S}_j) \\ &\quad - \sum_i \mu_i \mathbf{B}_{\text{ext}} \cdot \mathbf{S}_i + \sum_i K_{\text{ani}}^U (\mathbf{S}_i \cdot \mathbf{e}_z)^2. \end{aligned} \quad (1)$$

Here,  $\mathbf{S}_i$  is the classical Heisenberg spin at site  $i$  (*i.e.*, expressed as a three-dimensional unitary vector),  $\mu_i$  is the magnetic moment associated with that site,  $\mathbf{B}_{\text{ext}}$  is the applied magnetic field,  $J_{ij}$  and  $\mathbf{D}_{ij}$  are the Heisenberg and Dzyaloshinskii–Moriya interactions, and  $K_{\text{ani}}^U$  represents the single-ion uniaxial anisotropy constant with respect to the easy axis  $\mathbf{e}_z$ . Each vector is constructed using three outputs from the neural network. In the present study of the Pd/Fe/Ir(111) system, we consider a 2D supercell composed by  $100 \times 100$  Fe spins ( $23.6 \times 27.2 \text{ nm}^2$ ) with periodic boundary conditions in the  $xy$  plane.

With the proposed mapping and parameterization of the spin system, the effective gradient-descent based learning algorithm can be used to perform the desirable minimization of the Hamiltonian function:

$$W^{(i)} = W^{(i-1)} - \frac{\partial \mathcal{H}}{\partial W}, \quad (2)$$

in which  $W$  is the weight of the neural network. Thus, the stopping condition for the iterative update of the network's weights is controlled by the threshold parameter  $T_s$ :

$$\mathcal{H}^{(i)} - \mathcal{H}^{(i-1)} < T_s, \quad (3)$$

where  $\mathcal{H}^{(i)}$  is the Hamiltonian value at the  $i$ -th checkpoint (typically gaped by 50 optimization steps) of the algorithm. Once the solution is found, *i.e.*, Eq. 3 is fulfilled, a new search for another solution is triggered by the following condition:

$$T_p^{\text{low}} < \mathcal{H}_p < T_p^{\text{high}}. \quad (4)$$

Here,  $T_p^{\text{low}}$  and  $T_p^{\text{high}}$  are the lower and higher perturbation thresholds, and  $\mathcal{H}_p$  is some in principle arbitrary combination of spin-Hamiltonian terms guided by physical insights of the system. In this work, since the Dzyaloshinskii–Moriya interaction is one of the central interactions for the formation of topological spin textures in Pd/Fe/Ir(111), we have selected to use the Dzyaloshinskii–Moriya terms as  $\mathcal{H}_p$ :

$$\mathcal{H}_p = \sum_{i \neq j} \mathbf{D}_{ij} \cdot (\mathbf{S}_i \times \mathbf{S}_j). \quad (5)$$

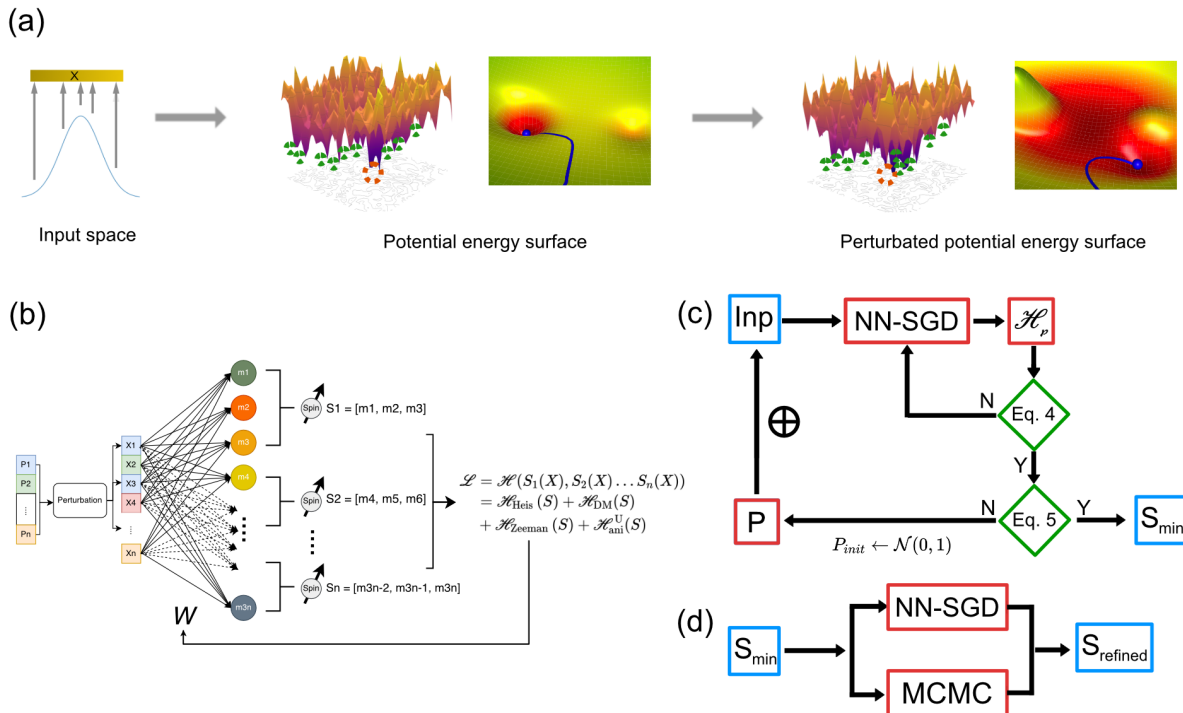


Figure 1. (Color online) (a) Conceptual illustration of how the algorithm uses the loss landscape of the perturbed shallow neural network (NN) to find local minima, *i.e.* metastable spin configurations. The left-most image illustrates that the input space  $X$  is sampled from a Gaussian distribution. The next image represents a schematic view of a complex (rugged) PES with many local minima, whose positions are indicated by the green dotted circles. The red dotted circle indicates the position of the global minimum. The middle image illustrates a small part of the PES. Here, red (yellow) color indicates a low (high) energy. The blue line shows how our algorithm converges toward a local minimum using the stochastic gradient descent (SGD) method. The next image shows a perturbed PES, in which the relative depths of the minima have been changed. Finally, the right-most image shows a small part of the perturbed PES and how our algorithm now converges toward another minimum. (b) Chart of the feed-forward perturbed NN subject to a random input perturbation. (c) Workflow of the NN. Inp, P,  $S_{\min}$  and NN-SGD refer, respectively, to the NN's input, random perturbation process, the spin configuration found to minimize the Hamiltonian  $\mathcal{H}_p$  (loss function), and the NN's loss minimization by SGD. (d) Workflow of the NN-SGD based algorithm hybridized with NN-SGD and MCMC to refine the search for the spin configuration.  $S_{\min}$  refers to the solution found by the NN loss minimization up to an intermediate threshold, and  $S_{\text{refined}}$  is the solution refined by NN-SGD and Metropolis MCMC optimizer. The pseudocode for workflow (c) can be found in Appendix VII A.

In essence, as shown in Figure 1 (c), the search is initiated with a heuristic perturbation of the inputs (initial conditions) by a random process drawn from a Gaussian distribution  $P \sim \mathcal{N}(0, 1)$ . The result of this procedure is that we make a *random jump* in the PES. However, due to our choice of  $\mathcal{H}_p$ , the resulting new random starting-point spin configuration should be relevant from a physical point of view. A further issue is that we want to sample as many different parts as possible of the PES. Therefore we deliberately select each new random spin configuration (which we reach with our *random jumps*) to be dissimilar to each other. In practice, this is done by creating many different randomized spin configurations (typically about 200) and from these, select the one most dissimilar to the previously addressed spin configuration. This procedure is then followed by a search for the nearest-lying local minimum. This search can be done in several ways. In this work, we have selected

to try out two local optimization schemes — the first one is a stochastic gradient descent (SGD) method called AdamW [30, 31](NN-SGD in Fig. 1 (c)), and the second one is a non-gradient method based on Markov Chain Monte Carlo (MCMC). We will in the following denote the first as the *independent mode* and the latter method as the *hybrid mode*. The independent mode is called in this way because it simply uses the gradient descent inherent in the NN algorithm. On the other hand, as it will be detailed in Section II C, at some point during the search in the hybrid mode we switch from the NN gradient descent to MCMC.

Basically, the Metropolis MCMC optimizer (as implemented in the UppASD software [22]) performs energy minimization under finite temperatures by using the transition probability  $P_t$  between two spin configurations in a Markov chain:

$$P_t = \begin{cases} \exp\left(-\frac{\Delta E}{k_B T}\right), & \text{if } \Delta E > 0 \\ 1, & \text{otherwise} \end{cases}, \quad (6)$$

where  $\Delta E$  is the energy difference between the spin configurations,  $k_B$  is the Boltzmann constant, and  $T$  is the temperature of the system.

When the hybrid mode is used, a less strict condition for the network convergence, *i.e.*, a higher (or *intermediate*) value of the threshold hyperparameter  $T_s$  can be adopted.

### B. Computation of the spin Hamiltonian parameters

The electronic structure calculations of the fcc-Pd/Fe/Ir(111) multilayer system were performed in the framework of the Density Functional Theory (DFT). Here we used the self-consistent real-space linear muffin-tin orbital method in the atomic-sphere approximation (RS-LMTO-ASA) [32, 33] with the local spin density approximation (LSDA) exchange-functional [34]. The resulting *ab-initio* magnetic moments, as well as coupling parameters  $J_{ij}$  and  $\mathbf{D}_{ij}$ , used in Eq. 1, were described in detail in Ref. [35]. To avoid effects coming from anticipated truncation, the coupling coefficients were considered up to 360 neighbors (within a distance of  $\sim 7a$  from the reference site, where  $a = 3.84 \text{ \AA}$  is the experimental lattice parameter of the Ir host). In turn, the experimental value (0.4 meV/Fe [36]) is here assumed for the  $K_1^U$  uniaxial anisotropy constant. Concerning the Zeeman term in Eq. 1, we set the external field to be  $B_{ext} = 3.5 \text{ T}$  and applied to the out-of-plane direction ( $[001]$ ). At this field, similarly to situation depicted in Ref. [20], the skyrmion lattice and ferromagnetic (single-domain) solutions are energetically almost degenerate [35], being isolated skyrmions characterized as metastable structures. Finally, for the Gilbert damping parameter in SLLG, we used the value  $\alpha \sim 0.01$ , which is in the order of magnitude of the intrinsic  $\alpha$  in thin films (lower limit) [37].

In the approximation where the Pd-induced spin moments are treated as independent degrees of freedom [38], the Pd layer (when considered explicitly in the ASD simulations) reproduces the Fe layer spin texture [35]. Therefore, we restrict ourselves to the analysis of the Fe layer.

The total topological charge,  $Q_{total}$ , of each spin configuration was calculated using the discrete method proposed by Berg and Lüscher [39], with periodic boundary conditions. The quantity  $Q_{total}$  accounts for all topological structures with individual winding numbers  $Q_i$  in the spin system ( $Q_{total} = \sum_i Q_i$ ), which can be isolated for the evaluation of the respective charges.

### C. Practical comparison between the *independent* and *hybrid* modes

For spin configurations that represent a sufficiently deep local minimum in the PES – *i.e.*, that the energy barrier is higher than a given threshold  $T_s$  ( $\Delta E > T_s$ , see Eq. 3) – the functional implementation of the NN defined in Section II A can benefit from the so-called *hybrid* mode. Although we cannot compare directly the efficiency of both algorithms (NN gradient descent and MCMC), as, among other reasons, they use different architectures (GPU and CPU parallelized by OpenMP, respectively), and are written in different programming languages, we can confront the execution times of the independent and hybrid modes from the *user* perspective.

To achieve this practical comparison, we set an intermediate threshold in the context of Eq. 3 ( $T_s^{\text{int}} = 10^{-3} \text{ mRy/atom}$ ) for the point from where the MCMC (hybrid mode) or the NN gradient descent (independent mode) algorithm will continue the energy minimization process up to a final threshold  $T_s^{\text{final}} = 10^{-6} \text{ mRy/atom}$ . In both cases, the magnetic textures eventually converge to the same configuration on the PES, but with distinct execution times. Typical optimization procedures for the independent and hybrid modes, for different initial spin configurations, are shown in Fig. 2(a) and (b), respectively. Within the hybrid scheme, we reach only a certain point on the way to the local minimum (*i.e.*, in an advised convex hull) before changing to MCMC, marked with a yellow dashed circle in Fig. 2(b). In Fig. 2 (a/b), the blue dashed circle in the right lower corner denotes the time in which the minimization process reached  $T_s^{\text{final}}$ . In turn, the green dashed circle represents the perturbation operation where an undesirable local minimum is found (*i.e.*, that do not fulfills Eq. 4).

In Fig. 2 (c), we compare the execution times of the two approaches for ten randomly selected initial spin configurations. In order to produce a fair comparison, both algorithms (NN gradient descent and MCMC) start at  $T_s^{\text{int}}$  from the same point within each case, stopping the minimization procedure at  $T_s^{\text{final}}$ . The red (green) dots show the execution times, counted from the intermediate threshold, for the independent (hybrid) modes. As can be seen, the hybrid scheme shows consistently shorter execution times.

### D. Atomistic spin dynamics simulations

For the stability analysis of the textures found by the proposed algorithm in this work, we solve the stochastic Landau-Lifshitz-Gilbert (sLLG) equation [22], which is implemented in the Uppsala Atomistic Spin Dynamics (UppASD) package [40], and is given as:

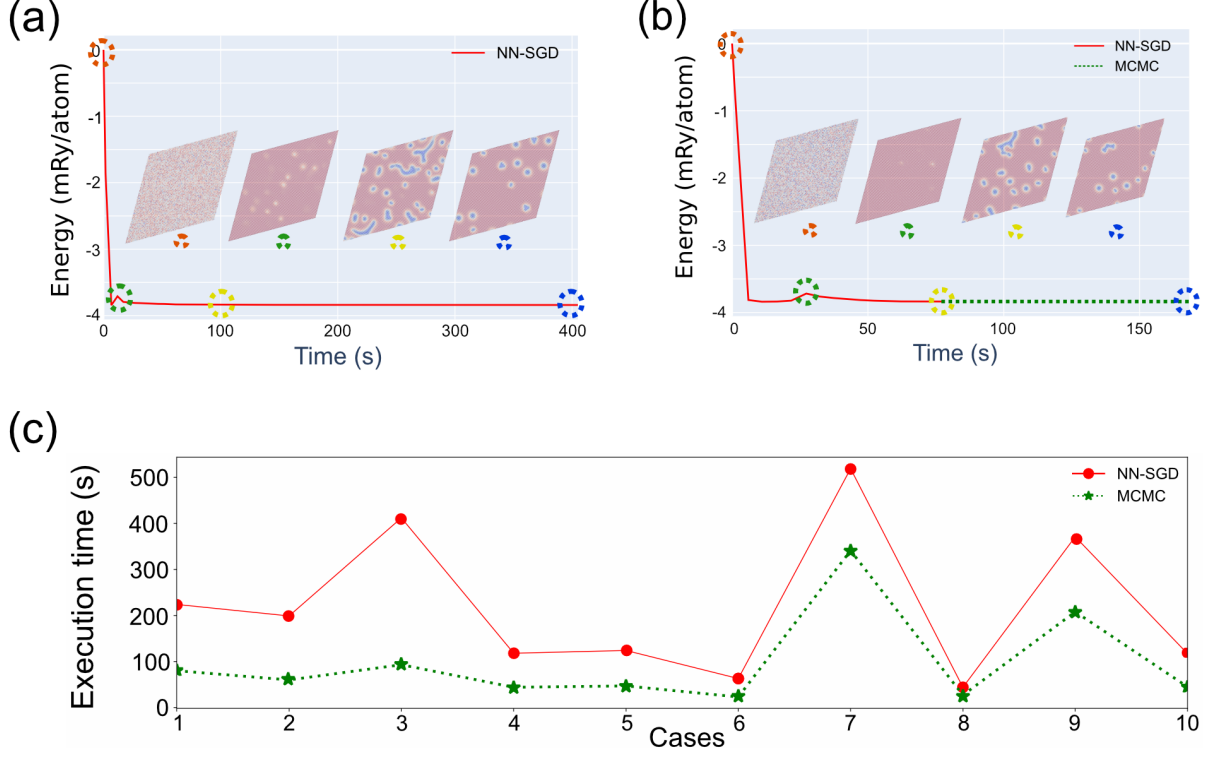


Figure 2. (Color online) Illustration of (a) independent (NN-SGD), (b) hybrid modes (NN-SGD + MCMC), and (c) execution times comparison between them, from the user perspective. Panels (a/b) show only a schematic representation of the optimization procedures (see text), starting from different spin configurations. As such, they should not be viewed in a comparative way. The red, green, yellow, and blue circles represent the starting point (random spin texture), the perturbation operation when an undesirable local minimum (*i.e.* that do not fulfills Eq. 4) is found, the point where the NN gradient descent reaches the intermediate threshold (advised convex hull) of  $T_s^{\text{int}} = 10^{-3}$  mRy/atom (see Eq. 3), and the point where the final threshold of  $T_s^{\text{final}} = 10^{-6}$  mRy/atom is reached, respectively. When the minimization process arrives at  $T_s^{\text{int}}$ , in the hybrid mode we switch from the neural network build-in gradient-descent-based optimization scheme to the MCMC scheme. In turn, panel (c) shows the execution times (see text) of both algorithms, for ten randomly selected cases. The neural network optimization was performed on a single Nvidia A100 GPU, whereas the built-in MCMC optimization used an Intel Xeon Gold 6130 CPU, parallelized with OpenMP. The parallelogram insets in both subplots (a/b) represent the magnetic textures of the system at different times during the minimization procedure. Illustrative movies of the optimization processes can be found in the Supplementary Material.

$$\begin{aligned} \frac{d\mathbf{m}_i}{dt} = & -\gamma_L \mathbf{m}_i \times (\mathbf{B}_i + \mathbf{B}_i^f) \\ & -\gamma_L \frac{\alpha}{m_i} \mathbf{m}_i \times [\mathbf{m}_i \times (\mathbf{B}_i + \mathbf{B}_i^f)], \end{aligned} \quad (7)$$

where  $\mathbf{B}_i = -\frac{\partial \mathcal{H}}{\partial \mathbf{m}_i}$  is the effective field on site  $i$ , related to the Hamiltonian defined in Eq. 1 and parametrized by the *ab-initio* quantities described in Section II B. The dimensionless (and isotropic) Gilbert damping parameter is here denoted by  $\alpha$ , while  $\gamma_L = \frac{\gamma}{(1+\alpha^2)}$  is the renormalized gyromagnetic ratio (as a function of the bare one,  $\gamma$ ). In turn,  $\mathbf{B}_i^f$  is the stochastic field arising from the

thermal fluctuations. This term describes how temperature effects are considered in the spin dynamics, in a Langevin approach [40].

In Eq. 7, the first term express the precessional motion of atomistic magnetic moments in a given system, and the second term describes the damped motion (both in the adiabatic approximation, *i.e.*  $\frac{d|\mathbf{m}_i|}{dt} = 0$ ). Besides the dynamics, in the absence of thermal effects, the solution of Eq. 7 with  $\alpha > 0$  corresponds to the relaxation process of finding the nearest energy minimum in the PES.

Throughout the text, we define the typical simulation times of 200 ps (for the stability of the topological charge) and 2 ns (for the calculation of the average energy/spin

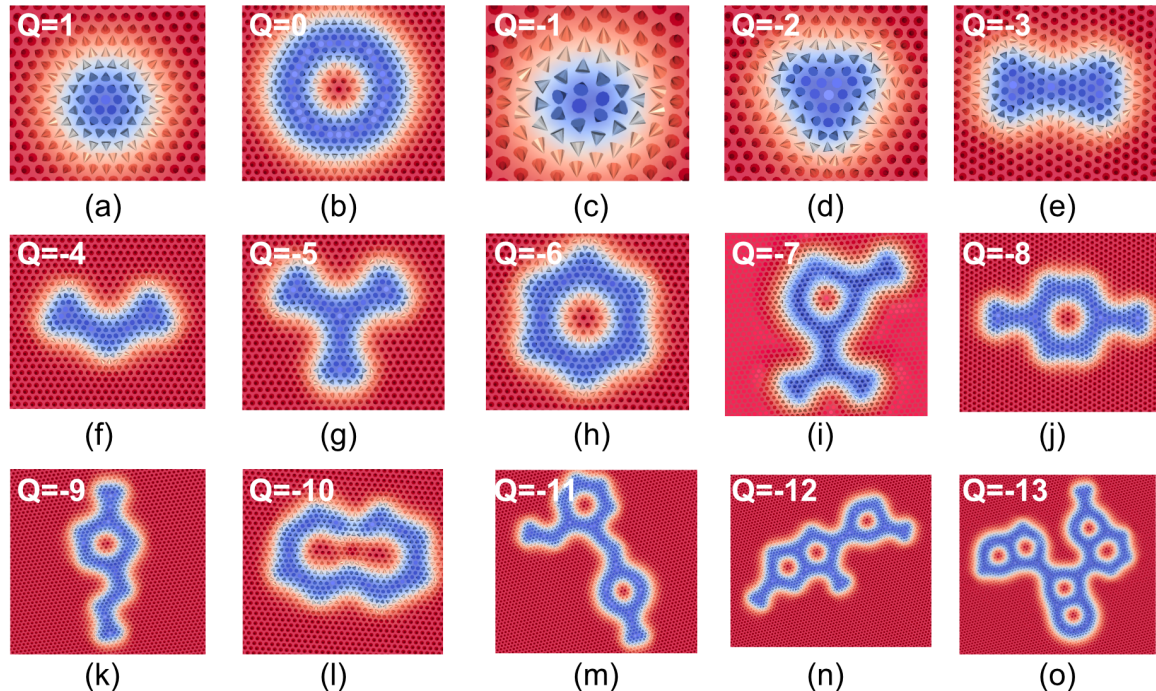


Figure 3. Identified topological metastable spin textures by our NN-MCMC hybrid method in the Pd/Fe/Ir(111) system with  $B_{ext} = 3.5$  T. (a) skyrmion, (b) skyrmionium, (c) antiskyrmion, (d) to (o): isolated magnetic textures, with higher-order topological charge varying between  $Q = -2$  and  $Q = -13$ . The distance between neighboring spins (cones) is  $a\frac{\sqrt{2}}{2} \sim 2.72$  Å. Blue and red colors indicate opposite spin directions.

with  $T > 10^{-4}$  K). The numerical solution of Eq. 7 is obtained with a time step of  $\Delta t = 10^{-16}$  s.

### III. RESULTS

#### A. Textures with higher-order $Q$

The NN-MCMC hybrid model was applied to systematically explore unusual topological magnetic textures in the fcc-Pd/Fe/Ir(111) system. In Fig. 3, we show 15 isolated spin configurations that have been identified to be metastable by the current algorithm, with the topological charge number  $Q$  varying from 1 to  $-13$ .

We note that the positive  $Q$  textures (with  $Q > 1$ ), whose morphology can be characterized by the so-called *skyrmion bags* [12] (see Appendix VIIC), were not directly found in our simulations; they, however, also represent (metastable) solutions that can be stabilized by manual crafting of the initial state. This crafting process is analogous to that reported in Ref. [12], in which a closed  $2\pi$  domain wall is filled inside with  $N$  skyrmions ( $Q = 1$  structures). By relaxation of the spin matrix, the domain wall tends to shrink down to the skyrmionium size, whose dynamics is blocked by the interparticle repulsion with skyrmions and results in a stable skyrmion

bag with  $Q = N$ . The fact that the positive  $Q$  solutions were not found by a direct PES search can be in part understood in terms of the intrinsic preference of skyrmions over antiskyrmions by Pd/Fe/Ir(111), imposed by the DMI, which leads to a well-known skyrmion lattice ground-state for a range of applied  $B$  [15, 35], and a higher stability of the former with respect to the latter. This higher stability of skyrmions is expressed in at least two ways: (i) a relatively high temperature to measure a topological charge decay within 200 ps (here calculated to be  $T \sim 55$  K) compared to its counterpart; and (ii) a minimum energy path to collapse with an enhanced energy barrier with respect to antiskyrmions (see Appendix VIIB). Thus, skyrmion-based structures are expected to have higher activation energy barriers with respect to the ferromagnetic/single-domain (ground) state, at  $B_{ext} = 3.5$  T, than antiskyrmion-based textures; those skyrmion-based textures also present enhanced relative energies (w.r.t. the field-polarized state) compared to their opposite- $Q$  counterparts. The lack of positive  $Q$  solutions by direct search motivated here the more focused analysis of the negative  $Q$  branch.

It is also noteworthy that the existence of some higher-order  $Q$  shown in Fig. 3 (specially for  $|Q| > 6$ ) has a sensitive dependence on the exchange frustration, *i.e.*, on the relation  $\frac{|J_3|}{J_1}$  – where  $J_n$  denotes the Fe-Fe in-

interaction from a reference site to its  $n$ -th neighboring shell  $-$ , and a change of  $\sim 10\%$  in  $\frac{|J_3|}{J_1}$  can lift their theoretical metastability. This fact can be partially understood in terms of the role played by the frustration of the isotropic exchange interactions, which can be responsible for the presence of energy minima with attractive character in the antiskyrmion-antiskyrmion interaction potential [16]. Therefore, given favorable conditions (such as the magnitude of the applied magnetic field), we find that this 2D layer system can hold spin textures like skyrmion, skyrmionium, antiskyrmion and high-order topological charge antiskyrmions resembling bags, and antiskyrmion bags including those similar to the ones obtained in other systems [18]. Some magnetic textures can also hold skyrmionium bags (see Fig. 3-(h)), skyrmionium bags with limbs (see Fig. 3-(i),(j),(k)) as well as bi-skyrmionium bags (see Fig. 3-(n),(o)).

### B. Stability analysis and binding energies

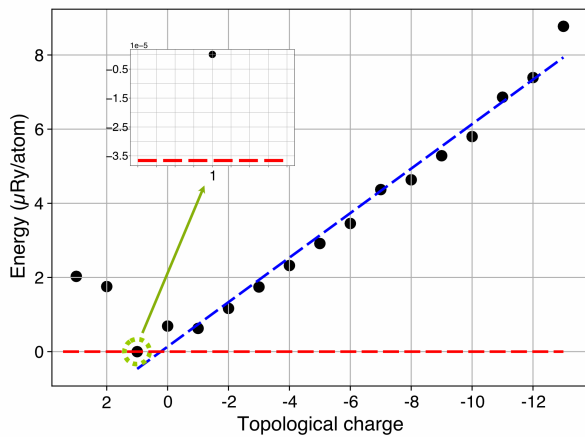


Figure 4. Relative energy per atom of isolated spin textures with topological charge  $Q$  ranging from  $-13$  to  $1$ , also including the  $Q = +2$  and  $Q = +3$  cases. The total energy is calculated by embedding each topological excited state in an fcc-Pd/Fe/Ir(111) supercell i.e., a single-domain ferromagnetic background with size  $23.6 \times 27.2 \text{ nm}^2$ . The energy scale in the figure is set so that the lowest energy (i.e., the  $Q = 1$  skyrmion state) is zero, for visibility. The black dots are computed energies and the blue dashed line is a linear fit to the data. The horizontal red dashed line shows the energy of the ferromagnetic state. The inset shows the energy gap between  $Q = -1$  and the ferromagnetic state.

Generally speaking, for each charge  $Q$ , several spin textures are possible, with varying number of holes (i.e., non-self-intersecting curves that define the domain walls in the structure), and/or the so-called chiral kinks [19]. In Fig. 4, we choose the lowest-energy topological spin texture of the respective  $Q$  found in our simulations (at  $B_{ext} = 3.5 \text{ T}$ ), and show the computed energy difference with respect to the ferromagnetic single-domain state

( $Q = 0$ ),  $\Delta E = E - E_{\text{FM}}$ . We see that the energy difference,  $\Delta E$ , is almost linear with respect to  $Q$ , with a slope that increases with the applied magnetic field. For the particular  $B_{ext}$  considered here, as  $Q$  decreases one unit, the energy per spin increases on average  $\sim 0.6 \mu\text{Ry}$ . Consequently, the antiskyrmion states with  $|Q| \geq 1$  are relatively close in energy.

To gain a more detailed understanding of the stability and lifetimes of these topological spin textures, we performed atomistic spin dynamics simulations using the UppASD software package [22]. Figure 5 depicts the results from these simulations for selected topological spin textures with a  $Q$  ranging from  $-3$  to  $-6$ . Based on the topological charge decay time  $\tau$  (i.e., the time intervals in which the spin textures change their initial  $Q$  values), final topological charges, final magnetic moment (per site), and also visual inspection, we divided the charts into four basic zones. Before characterizing them, however, it is worth to define the *binding energy* of a given high-order skyrmionic texture,  $E_b(Q)$ . With the assumption that every high-order (anti)skyrmion (that does not present a hole) is an excited state consisting of multiple bounded  $Q = \pm 1$  structures, we can define  $E_b(Q)$  as [17]

$$E_b(Q) = E(Q) - |Q| E(\text{sign } Q), \quad (8)$$

$$\text{where } E(\text{sign } Q) = \begin{cases} E(Q = -1), & \text{if } Q < 0 \\ E(Q = 1), & \text{if } Q > 0 \end{cases}.$$

With this definition, the binding energies of the HO-ASk with  $Q \in [-5, -3]$  are given in Table I. The negative values obtained for  $E_b$  indicate the trend for lower- $Q$  structures to combine together forming a more complex structure with higher total  $Q$ . This, together with the facts that (i) single antiskyrmions are stable up to sizable temperatures ( $T \sim 32 \text{ K}$  at  $B_{ext} = 3.5 \text{ T}$ ), which makes the population of these metastable states more likely (with a finite probability given by the Boltzmann factor); and (ii) HO-ASk are relatively close in energy (Fig. 4), suggests that some high- $Q$  states in Pd/Fe/Ir(111) can be formed experimentally, at their critical temperatures, by merging of  $Q = -1$  textures, as similarly proposed in Ref. [41]. The process of bound states generation, however, should overcome an energy barrier. As Table I shows,  $E_b$  increases with temperature, enhancing also the chance that high- $Q$  structures separate into lower- $Q$  (or unitary- $Q$ ) constituents due to thermal effects.

Thus, zone I indicates the region in field and temperature in which the topological quasi-particles are stable ( $\tau > 200 \text{ ps}$ ), keeping their initial real-space structure intact. When  $B$  and/or  $T$  becomes sufficiently high to reduce the binding energy (see Eq. 8) by favoring the FM state or due to thermal fluctuations, these HO-ASk unpack in lower- $Q$  textures. Such lower- $Q$  structures can now be stable or survive for only few picoseconds – when  $k_B T$  becomes progressively comparable with the respective collapse energy barriers. This characterizes the transition region (zone II), where the initial HO-ASk are unstable but topological quasi-particles are still

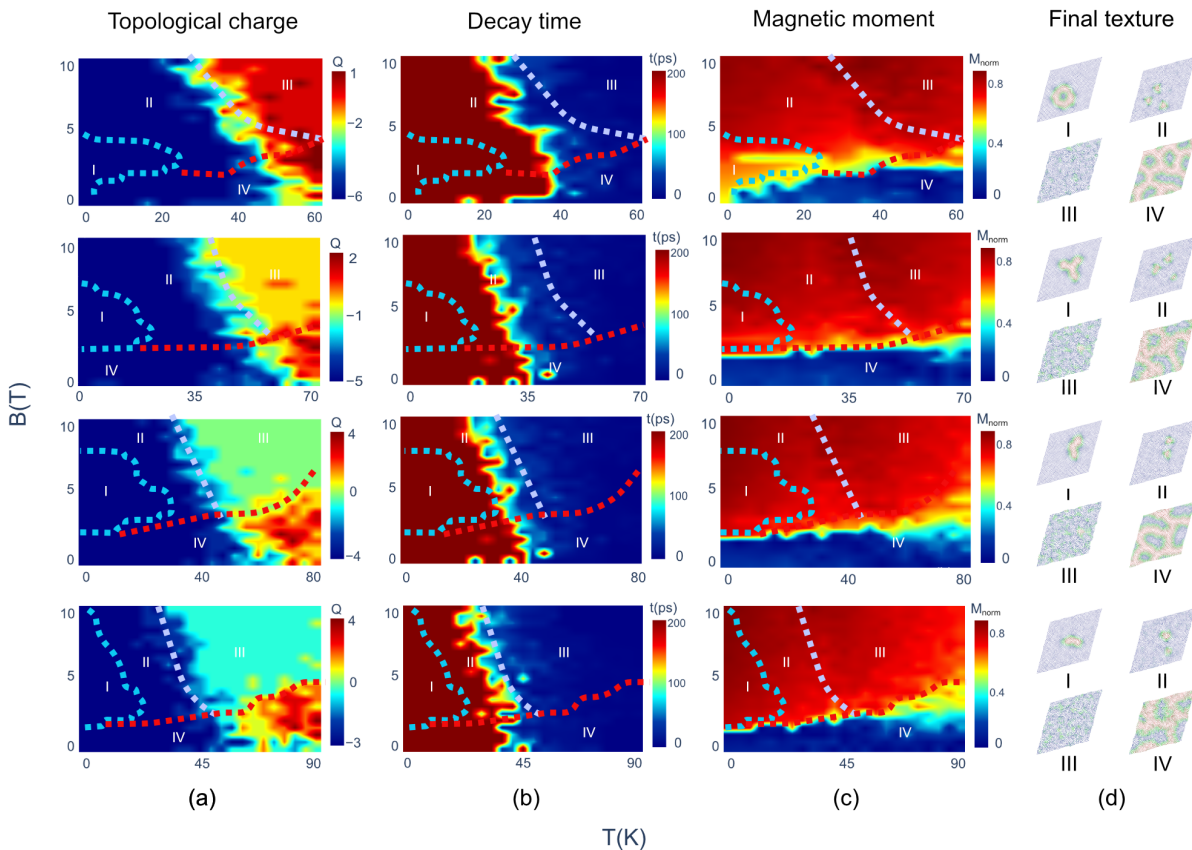


Figure 5. Magnetic field versus temperature stability maps of antiskyrmions with topological charge varying from  $Q = -3$  up to  $Q = -6$ . Columns 1 to 3 show the final topological charge, topological charge decay time and the normalized magnitude of the final magnetic moment, respectively. The top row is for  $Q = -6$ , the second row is for  $Q = -5$ , the third row is for  $Q = -4$  and the bottom row is for  $Q = -3$ . In the right-most column we show the magnetic textures in each zone (I, II, III and IV) predicted by the NN-MCMC hybrid model.

present. With further increasing temperature, even the lower- $Q$  textures become unstable, gradually shifting to a mostly FM spin configuration (note that here  $T \lesssim T_C$  [35]), which defines zone III. Finally, in zone IV we find metastable configurations which resemble domain structures. In that zone, the sufficiently low  $B$  either drives the spin-spiral to be the ground-state, or a competition between spin-spiral and skyrmion lattice as the lower-energy state. As a general trend, we notice that the region where the HO-ASk are stable (zone I) diminishes with increasing initial  $|Q|$ .

The definition of  $E_b$  also clarifies, by another point of view, the absence of  $Q \geq 2$  solutions in our direct PES search with both the perturbation-driven neural network and the simulated annealing methods; in this case, due to high-order skyrmions morphology, Eq. 8 is modified to account also for the skyrmionium energy:  $E_b(Q) = E(Q) - |Q| E(\text{sign } Q) - E(Q = 0)$ . As  $E(Q = 1)$  is one order of magnitude smaller than  $E(Q = -1)$ , a *positive* binding energy arises (see Table I for the example of  $Q = +2$ ). In other words, the given  $(B, T)$  conditions dictate no tendency of lower- $Q$  structures to generate more complex structures with a higher positive- $Q$ ,

which is corroborated by the skyrmion-skyrmion mutual repulsion.

### C. Geometry-topology analysis

We also calculate the energy difference between different spin textures of antiskyrmions with higher-order topological charge. As shown in Fig. 6, the spin textures have different energy even though all of them have the same topological charge ( $Q = -5$ ). The structures can be classified into three different groups. The textures shown in Figs. 6 (b)-(d) can be described as skyrmioniums with different number and lengths of limbs and in Fig. 6 (e) the texture resembles skyrmionium bags while the remaining plots represent antiskyrmions (Figs. 6(f)-(h)). Overall, the skyrmionium textures have higher energy and, consequently, are less stable than the ones without holes inside. This result was already observed in Figs. 3 and 4 where the spin textures with holes are more prone to appear when the topological charge is large and, consequently, with less stability as compared to the structures with low topological charge.



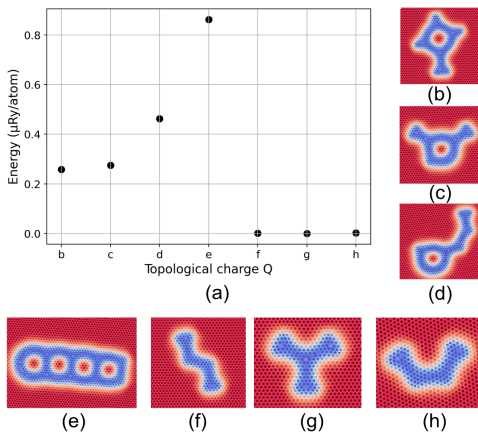


Figure 6. (a) Relative energy, with respect to the ferromagnetic single-domain state, per atom of the isolated topological textures with topological charge  $Q = -5$  in a magnetic field of 3.5 T, shown in panels (b) to (h). The energy scale here is set so that the energy is zero for the texture with the lowest energy per atom.

#### IV. SUMMARY AND CONCLUSION

In this study, we first proposed a heuristic metastable state searching algorithm based on perturbed neural work. We used the landscape of the loss space, where the loss function is the spin Hamiltonian itself, which represents the real potential energy surface. Then, a gradient-based independent mode and a hybrid mode, which introduced the MCMC optimizer, are presented for quick searching. Finally, we illustrated the effectiveness of the proposed algorithm by heuristically exploring long-life metastable states in the Pd/Fe/Ir(111) system. It is worthwhile to mention here that the efficiency of the algorithm can be improved by designing optimal stop conditions. We also compared the execution time of the MCMC algorithm (denoted above as the hybrid mode) with respect to the NN gradient descent algorithm (denoted above as the independent mode) and we found that the hybrid scheme is consistently shorter in execution time with respect to the independent mode. This result paved the way to use the MCMC algorithm in cases where the execution time plays an important role like large system size or number of exchange couplings between atoms.

Based on the hybrid method described above, it is able to predict a myriad of topological metastable spin textures as shown in Fig. 2. The results also show that in the Pd/Fe/Ir(111) system, high-order antiskyrmions and skyrmionium bags have more chance to exist than skyrmion bags due to their stability. As aforementioned, some solutions that we find are not reported yet, e.g., the texture in Fig. 3 (l). Finally, we applied spin dynamic simulation at finite temperatures and calculated binding energy to study the stability of those novel textures, so that, the relative energy per atom of the studied isolated

Table I. Energies  $E(Q)$  of the topological structures with respect to the ferromagnetic (single-domain) background, and binding energies  $E_b(Q)$  of HO-ASk (see Eq. 8), both given in  $\mu\text{Ry/atom}$ . The out-of-plane applied field is  $B = 3.5$  T, at the temperatures indicated in parenthesis.

$Q$	$E(Q)$	$E_b(Q)$
+1	0.04 ( $< 10^{-4}$ K)	n.d. <sup>a</sup>
	0.04 (3 K)	
	0.04 (20 K)	
-1	0.67 ( $< 10^{-4}$ K)	n.d.
	0.67 (3 K)	
	0.67 (20 K)	
-3	1.78 ( $< 10^{-4}$ K)	-0.22
	1.79 (3 K)	-0.21
	1.80 (20 K)	-0.20
-4	2.36 ( $< 10^{-4}$ K)	-0.31
	2.36 (3 K)	-0.30
	2.42 (20 K)	-0.25
-5	2.95 ( $< 10^{-4}$ K)	-0.39
	2.95 (3 K)	-0.37
	3.02 (20 K)	-0.31
+2	1.76 ( $< 10^{-4}$ K)	0.94
	1.76 (3 K)	0.95

<sup>a</sup> n.d. = not defined

spin textures is almost linear with respect to the topological charge. Based on the calculated linear trend and the negative binding energies found for antiskyrmions with high order  $Q$ , we predict that those spin textures shown in Fig. 3 are very likely to be found in experiments. In summary, we constructed a flexible and practical procedure that can explore PES for searching metastable states with a perturbation-driven neural network. This algorithm is applied to the Pd/Fe/Ir(111) system and discovered several novel spin textures. The current study will open a new avenue for future research that focuses on unconventional spin textures and long-life metastable states in materials with long-range interactions.

#### V. DATA AVAILABILITY

All data is available from the authors upon reasonable request.

#### VI. CODE AVAILABILITY

All the relevant code is available from the authors upon request.

## ACKNOWLEDGMENTS

The authors acknowledge financial support from the Knut and Alice Wallenberg Foundation (KAW) through Grant No. 2018.0060. Q.X. acknowledges China Scholarship Council (201906920083). A.B. and O.E. acknowledge eSSENCE. A.D. acknowledges financial support from the Swedish Research Council (VR) through Grants No. 2019-05304 and 2016-05980. O.E. acknowledges support by the Swedish Research Council (VR), the Foundation for Strategic Research (SSF), the European Research

Council (854843-FASTCORR) and STandUP. D.T. acknowledges support from the Swedish Research Council (VR) with grant No. 2019-03666. E.S. acknowledges financial support from the Swedish Research Council (VR) through Grant No. 2017-03832. The computations/data handling were enabled by resources provided by KAW (Berzelius-2022-141) and the Swedish National Infrastructure for Computing (SNIC), partially funded by the Swedish Research Council through grant agreement No. 2016-07213. The authors also acknowledge discussions with Zhuanglin Shen.

- 
- [1] B. Kuhlman and P. Bradley, Advances in protein structure prediction and design, *Nature Reviews Molecular Cell Biology* **20**, 681 (2019).
- [2] G. L. Hart, T. Mueller, C. Toher, and S. Curtarolo, Machine learning for alloys, *Nature Reviews Materials* **6**, 730 (2021).
- [3] P. F. Bessarab, G. P. Müller, I. S. Lobanov, F. N. Rybakov, N. S. Kiselev, H. Jónsson, V. M. Uzdin, S. Blügel, L. Bergqvist, and A. Delin, Lifetime of race-track skyrmions, *Scientific reports* **8**, 1 (2018).
- [4] A. R. Oganov, C. J. Pickard, Q. Zhu, and R. J. Needs, Structure prediction drives materials discovery, *Nature Reviews Materials* **4**, 331 (2019).
- [5] A. Das and B. K. Chakrabarti, Colloquium: Quantum annealing and analog quantum computation, *Rev. Mod. Phys.* **80**, 1061 (2008).
- [6] M. Hervé, B. Dupé, R. Lopes, M. Böttcher, M. D. Martins, T. Balashov, L. Gerhard, J. Sinova, and W. Wulfhekel, Stabilizing spin spirals and isolated skyrmions at low magnetic field exploiting vanishing magnetic anisotropy, *Nat. Commun.* **9**, 1015 (2018).
- [7] S. Meyer, M. Perini, S. von Malottki, A. Kubetzka, R. Wiesendanger, K. von Bergmann, and S. Heinze, Isolated zero field sub-10 nm skyrmions in ultrathin co films, *Nat. Commun.* **10**, 3823 (2019).
- [8] H. Oike, A. Kikkawa, N. Kanazawa, Y. Taguchi, M. Kawasaki, Y. Tokura, and F. Kagawa, Interplay between topological and thermodynamic stability in a metastable magnetic skyrmion lattice, *Nat. Phys.* **12**, 62 (2016).
- [9] K. Karube, J. S. White, D. Morikawa, M. Bartkowiak, A. Kikkawa, Y. Tokunaga, T. Arima, H. M. Rønnow, Y. Tokura, and Y. Taguchi, Skyrmion formation in a bulk chiral magnet at zero magnetic field and above room temperature, *Phys. Rev. Mater.* **1**, 074405 (2017).
- [10] S. D. Yi, S. Onoda, N. Nagaosa, and J. H. Han, Skyrmions and anomalous hall effect in a dzyaloshinskii-moriya spiral magnet, *Phys. Rev. B* **80**, 054416 (2009).
- [11] N. Mohanta, E. Dagotto, and S. Okamoto, Topological hall effect and emergent skyrmion crystal at manganite-iridate oxide interfaces, *Phys. Rev. B* **100**, 064429 (2019).
- [12] F. N. Rybakov and N. S. Kiselev, Chiral magnetic skyrmions with arbitrary topological charge, *Phys. Rev. B* **99**, 064437 (2019).
- [13] B. Göbel, I. Mertig, and O. A. Tretiakov, Beyond skyrmions: Review and perspectives of alternative magnetic quasiparticles, *Phys. Rep.* **895**, 1 (2021), beyond skyrmions: Review and perspectives of alternative magnetic quasiparticles.
- [14] Z. Beheshti and S. M. H. Shamsuddin, A review of population-based meta-heuristic algorithms, *Int. J. Adv. Soft Comput. Appl* **5**, 1 (2013).
- [15] N. Romming, C. Hanneken, M. Menzel, J. E. Bickel, B. Wolter, K. von Bergmann, A. Kubetzka, and R. Wiesendanger, Writing and deleting single magnetic skyrmions, *Science* **341**, 636 (2013).
- [16] L. Rózsa, A. Deák, E. Simon, R. Yanes, L. Udvardi, L. Szunyogh, and U. Nowak, Skyrmions with attractive interactions in an ultrathin magnetic film, *Phys. Rev. Lett.* **117**, 157205 (2016).
- [17] L. Rózsa, K. Palotás, A. Deák, E. Simon, R. Yanes, L. Udvardi, L. Szunyogh, and U. Nowak, Formation and stability of metastable skyrmionic spin structures with various topologies in an ultrathin film, *Phys. Rev. B* **95**, 094423 (2017).
- [18] D. Foster, C. Kind, P. J. Ackerman, J.-S. B. Tai, M. R. Dennis, and I. I. Smalyukh, Two-dimensional skyrmion bags in liquid crystals and ferromagnets, *Nature Physics* **15**, 655 (2019).
- [19] V. M. Kuchkin, B. Barton-Singer, F. N. Rybakov, S. Blügel, B. J. Schroers, and N. S. Kiselev, Magnetic skyrmions, chiral kinks, and holomorphic functions, *Phys. Rev. B* **102**, 144422 (2020).
- [20] B. Dupé, C. N. Kruse, T. Dornheim, and S. Heinze, How to reveal metastable skyrmionic spin structures by spin-polarized scanning tunneling microscopy, *New Journal of Physics* **18**, 055015 (2016).
- [21] W. K. Hastings, *Monte Carlo sampling methods using Markov chains and their applications* (Oxford University Press, 1970).
- [22] O. Eriksson, A. Bergman, L. Bergqvist, and J. Hellsvik, *Atomistic spin dynamics: Foundations and applications* (Oxford university press, 2017).
- [23] P. F. Bessarab, V. M. Uzdin, and H. Jónsson, Method for finding mechanism and activation energy of magnetic transitions, applied to skyrmion and antivortex annihilation, *Comput. Phys. Commun.* **196**, 335 (2015).
- [24] G. P. Müller, M. Hoffmann, C. DiFelkamp, D. Schürhoff, S. Mavros, M. Sallermann, N. S. Kiselev, H. Jónsson, and S. Blügel, Spirit: Multifunctional framework for atomistic spin simulations, *Phys. Rev. B* **99**, 224414 (2019).
- [25] V. Roy, Convergence diagnostics for markov chain monte carlo, *Annual Review of Statistics and Its Application* **7**, 387 (2020).

- [26] I. Goodfellow, J. Pouget-Abadie, M. Mirza, B. Xu, D. Warde-Farley, S. Ozair, A. Courville, and Y. Bengio, Generative adversarial networks, *Communications of the ACM* **63**, 139 (2020).
- [27] Y. Miyatake, M. Yamamoto, J. Kim, M. Toyonaga, and O. Nagai, On the implementation of the 'heat bath' algorithms for monte carlo simulations of classical heisenberg spin systems, *J Phys C Solid State Phys* **19**, 2539 (1986).
- [28] N. Kawashima and J. Gubernatis, Loop algorithms for monte carlo simulations of quantum spin systems, *Physical review letters* **73**, 1295 (1994).
- [29] H. Li, Z. Xu, G. Taylor, C. Studer, and T. Goldstein, Visualizing the loss landscape of neural nets, *Advances in neural information processing systems* **31** (2018).
- [30] I. Loshchilov and F. Hutter, Decoupled weight decay regularization, arXiv preprint arXiv:1711.05101 (2017).
- [31] A. Paszke, S. Gross, F. Massa, A. Lerer, J. Bradbury, G. Chanan, T. Killeen, Z. Lin, N. Gimelshein, L. Antiga, *et al.*, Pytorch: An imperative style, high-performance deep learning library, *Advances in neural information processing systems* **32** (2019).
- [32] P. R. Peduto, S. Frota-Pessoa, and M. S. Methfessel, First-principles linear muffin-tin orbital atomic-sphere approximation calculations in real space, *Phys. Rev. B* **44**, 13283 (1991).
- [33] S. Frota-Pessoa, First-principles real-space linear-muffin-tin-orbital calculations of 3d impurities in cu, *Phys. Rev. B* **46**, 14570 (1992).
- [34] U. Von Barth and L. Hedin, A local exchange-correlation potential for the spin polarized case. i, *J. Phys. C: Solid State Phys.* **5**, 1629 (1972).
- [35] I. P. Miranda, A. B. Klautau, A. Bergman, and H. M. Petrilli, Band filling effects on the emergence of magnetic skyrmions: Pd/fe and pd/co bilayers on ir(111), *Phys. Rev. B* **105**, 224413 (2022).
- [36] J. Spethmann, E. Y. Vedmedenko, R. Wiesendanger, A. Kubetzka, and K. von Bergmann, Zero-field skyrmionic states and in-field edge-skyrmions induced by boundary tuning, *Commun. Phys.* **5**, 1 (2022).
- [37] E. Barati, M. Cinal, D. M. Edwards, and A. Umerski, Gilbert damping in magnetic layered systems, *Phys. Rev. B* **90**, 014420 (2014).
- [38] S. Polesya, S. Mankovsky, O. Sipr, W. Meindl, C. Strunk, and H. Ebert, Finite-temperature magnetism of  $\text{fe}_x\text{pd}_{1-x}$  and  $\text{co}_x\text{pt}_{1-x}$  alloys, *Phys. Rev. B* **82**, 214409 (2010).
- [39] B. Berg and M. Lüscher, Definition and statistical distributions of a topological number in the lattice  $O(3)$   $\sigma$ -model, *Nucl. Phys. B* **190**, 412 (1981).
- [40] B. Skubic, J. Hellsvik, L. Nordström, and O. Eriksson, A method for atomistic spin dynamics simulations: implementation and examples, *J. Phys. Condens. Matter* **20**, 315203 (2008).
- [41] U. Ritzmann, L. Desplat, B. Dupé, R. E. Camley, and J.-V. Kim, Asymmetric skyrmion-antiskyrmion production in ultrathin ferromagnetic films, *Phys. Rev. B* **102**, 174409 (2020).
- [42] S. von Malottki, B. Dupé, P. F. Bessarab, A. Delin, and S. Heinze, Enhanced skyrmion stability due to exchange frustration, *Sci. Rep.* **7**, 1 (2017).

## VII. SUPPLEMENTARY

### A. Pseudocode for the workflow

Pseudocode corresponding to the process illustrated in Fig.1c:

---

**Algorithm 1** Search for multi-stable spin configuration with a neural network

---

```

Set workflow stop condition  $T_S$ 
Set knowledge perturbation threshold  $T_P$ 
Set initial weight  $W_{init} \leftarrow \mathcal{N}(0, 1)$ 
Set initial bias of neural network  $B_{init} \leftarrow \mathcal{N}(0, 1)$ 
Apply random input vector of neural network  $X \leftarrow \mathcal{N}(0, 1)$ 
while  $\mathcal{H}_{NN}(current) > T_P$  do
  if  $\mathcal{H}_{NN}(current) - \mathcal{H}_{NN}(previous) > T_S$  then
    Minimize the loss  $\mathcal{L} = \mathcal{H}(S(X))$  via optimizer
  end if
end while
while  $\mathcal{H}_{NN}(current) < T_P$  do
  Randomly draw a perturbation vector  $P \leftarrow \mathcal{N}(0, 1)$ 
  Apply new input,  $X_{new}$  to the network,  $X \leftarrow X + P$ 
  while  $\mathcal{H}_{NN}(current) > T_P$  do
    if  $\mathcal{H}_{NN}(current) - \mathcal{H}_{NN}(previous) > T_S$  then
      Minimize the loss  $\mathcal{L} = \mathcal{H}(S(X))$  via optimizer
    end if
  end while
end while
Output spin configuration  $S \leftarrow$  shallow neural network ( $X$ )

```

---

### B. Minimum energy paths

The calculation of the minimum energy paths (MEPs) between two local minima in the energy surface results in the correspondent activation barrier. Considering one of

the states as the ferromagnetic (single-domain) configuration, then we can define the so-called path to *collapse*, and the resulting curve can be directly related to the stability of the topological texture.

Here, Geodesic Nudged Elastic Band (GNEB) method [23], as implemented in UppASD, is used in order to determine the MEP to collapse of a single skyrmion (or antiskyrmion) in Pd/Fe/Ir(111), considering the configuration space determined by the parameters described in Ref. [35]. The resulting MEPs are shown in Figure 7, where the highest activation barrier is obtained for the isolated skyrmion. This is consistent with previous calculations (*e.g.*, Ref. [42]), and demonstrates the enhanced stability of skyrmions in the context of annihilation to the ferromagnetic state.

### C. Real-space skyrmion bag textures

In Figure 8, we show the morphology of the metastable skyrmion bags stabilized at low temperatures at  $B_{ext} = 3.5$  T, and with relative energies w.r.t. the ferromagnetic (single-domain) state given in Fig. 4.

### D. Support movies

Examples of the energy minimization process and the resulting metastable state of Pd/Fe/Ir(111) containing high-order antiskyrmions, obtained with the use of the independent (hybrid) mode, can be found in Support Movies S1 (S2). In those movies, the frames in red and blue colors refer to the minimization from perturbed neural network, and gray and yellow frames are from MCMC, respectively. The red/gray colors represent the out-of-plane component of the magnetic moments, while the blue/yellow colors represent the in-plane components.

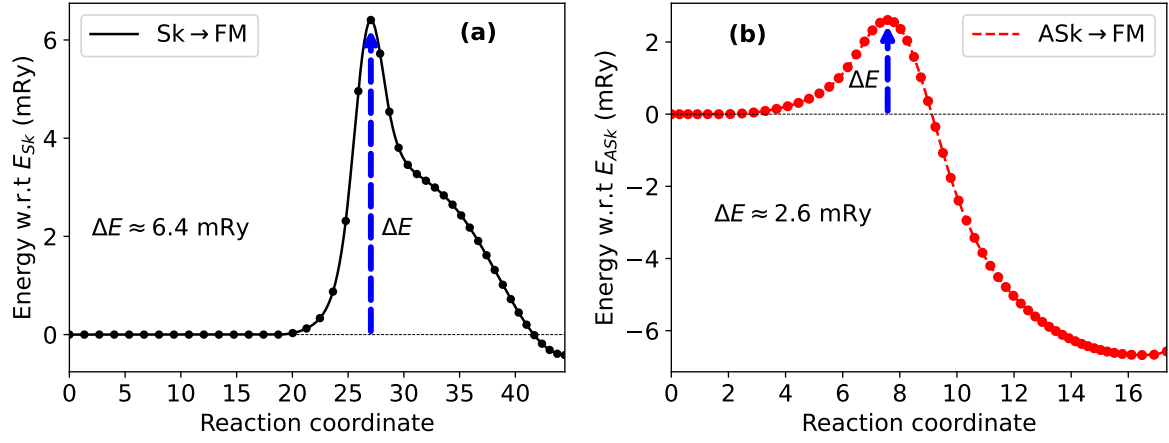


Figure 7. Minimum energy paths to collapse, at  $T = 10^{-4}$  K and  $B_{ext} = 3.5$  T, for: (a) single skyrmion; (b) single antiskyrmion on Pd/Fe/Ir(111). The energies are given with respect to the initial state (*i.e.*, isolated  $Q = \pm 1$  structure) and mapped as a function of the reaction coordinate corresponding to the collapse path to the ferromagnetic (FM) single-domain state. The maximum energy represents a first order saddle point in the potential energy surface.

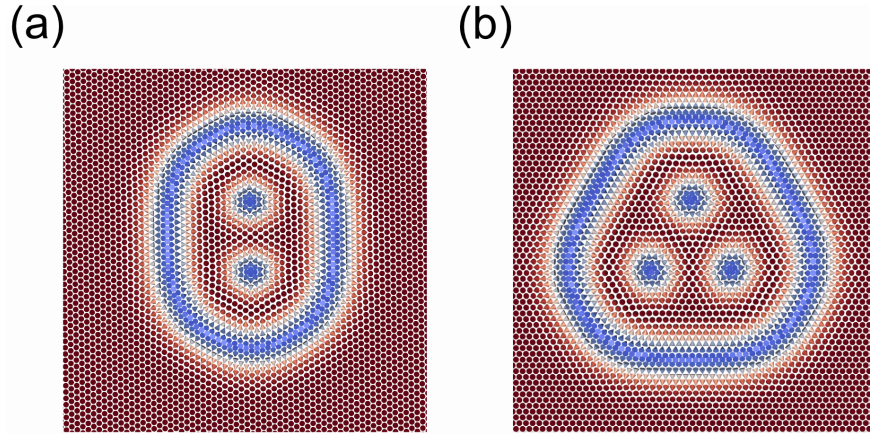


Figure 8. Morphology of metastable skyrmion bags in Pd/Fe/Ir(111) with topological charge: (a)  $Q = +2$ ; and (b)  $Q = +3$ , both stabilized with  $B_{ext} = 3.5$  T. The color schemes are the same as in Fig. 3.